Supplementary Information

Fe-Doping in Double Perovskite $PrBaCo_{2(1-x)}Fe_{2x}O_{6-\delta}$: Insights into Structural and Electronic Effects to Enhance Oxygen Evolution Catalyst Stability

Bae-Jung Kim [1,*], Emiliana Fabbri [1,*], Ivano E. Castelli [2], Mario Borlaf [3], Thomas Graule [3], Maarten Nachtegaal [1], Thomas J. Schmidt [1,4]

[1] Paul Scherrer Institut, Forschungstrasse 111, 5232 Villigen PSI, Switzerland
[2] Department of Energy Conversion and Storage, Fysikvej 309, Technical University of Denmark, DK-2800, Kgs. Lyngby, Denmark; ivca@dtu.dk
[3] Laboratory for High Performance Ceramics, Empa, Swiss Federal Laboratories for Materials Testing and Research, 8600 Dübendorf, Switzerland; mario.borlaf@empa.ch, thomas.graule@empa.ch
[4] Laboratory of Physical Chemistry, ETH Zürich, CH-8093 Zürich, Switzerland; thomasjustus.schmidt@psi.ch
* Correspondence: Bae-jung Kim joseph.kim@psi.ch; Tel.: +41-56-310-4580; Emiliana Fabbri emiliana.fabbri@psi.ch; Tel.: +41-56-310-2795

Table of Contents

S1. Brunauer-Emmett-Teller (BET) Surface Areas 1
S2. Density-Functional Theory Result: Pourbaix Diagram 2
S3. Lattice Parameters: Edge-sharing polyhedra and oxy(hydroxide) layer 3
S4. Operando FT-EXAFS Spectra Fittings 5
References 12

Table of Figures

Figure S1. Cyclic voltammetry and chronoamperometry measurements 2
Figure S2. Density-functional theory (DFT) calculated Pourbaix diagrams 3
Figure S3. Comparison of XANES spectra of PBC prepared via sol-gel (SG) vs. flame spray synthesis 4
Figure S4. Illustration of Co–Co distances 5
Figure S5. Comparisons of Co K-edge FT-EXAFS profiles with that of γ-Co-O(OH) 6
Figure S6. Comparison of FT Co K-edge EXAFS spectra collected during the operando XAS measurements 7
Figure S7. Fourier transformed k^3-weighted Co K-edge EXAFS spectra of PBC 9
Figure S8. Fourier transformed k^3-weighted Co K-edge EXAFS spectra of PBCF82 10
Figure S9. Fourier transformed k^3-weighted Co K-edge EXAFS spectra of PBCF55 11
Figure S10. Comparison of coordination number of the first peak of FT-EXAFS spectra 12

List of Tables

Table S1. Summary of BET surface areas of the prepared catalysts. 1
Table S2. Lattice Parameters of PrBaCo2(1-x)Fe2xO6-δ calculated from Rietveld refinement of X-ray diffractions 6
Table S3. Summary of best fit parameters of the FT k^3-weighted Co K-edge EXAFS spectra. 13

S1. Brunauer-Emmett-Teller (BET) Surface Areas

Table S1. Summary of Brunauer-Emmet-Teller (BET) surface areas of the prepared layered double perovskite catalysts.

Perovskite Oxide	BET Surface Area (m^2 g^{-1})
PBC	44
PBCF82	56
PBCF55	43

S2. Electrochemical Study

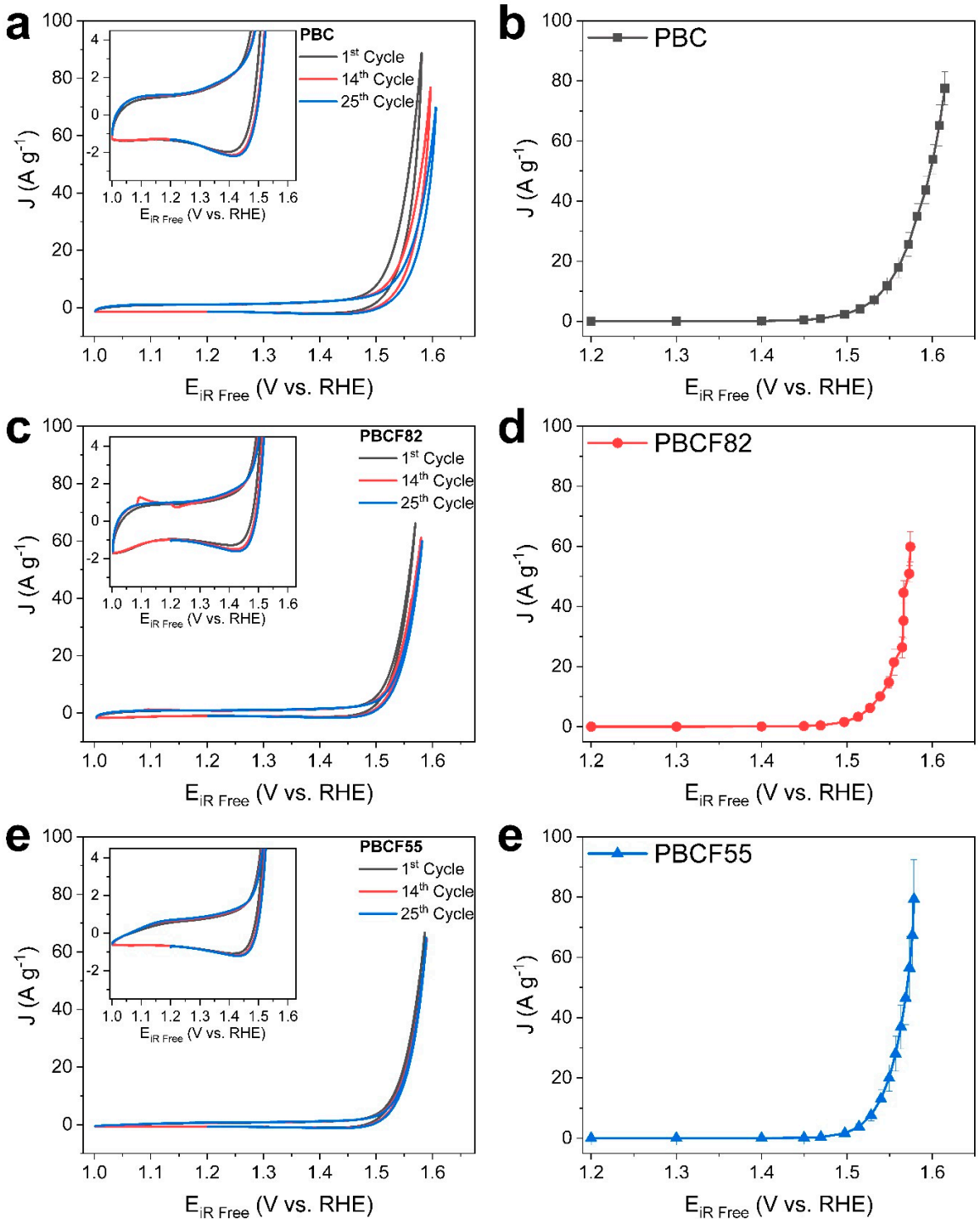

Figure S1. The initial cyclic voltammetry scanned at 10 mV sec^{-1} from 1.0 to 1.7 VRHE, and the series of chronoamperometry measurements recording steady-state current at each step of potential: a – b) PBC; c –d) PBCF82; and e – f) PBCF55.

S3. Density-Functional Theory Result: Pourbaix Diagram

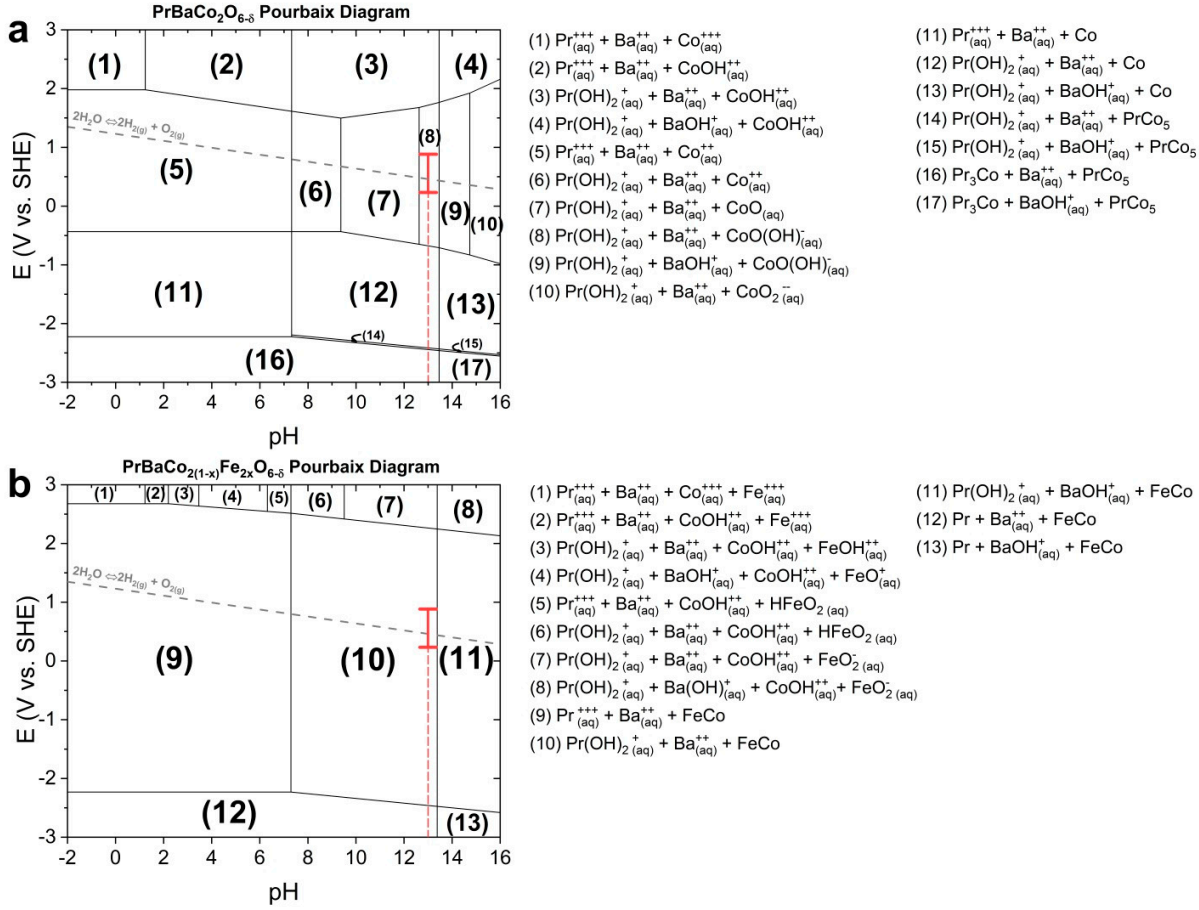

Figure S2. Density-functional theory (DFT) calculated Pourbaix diagrams of (a) $PrBaCo_2O_{6-\delta}$ and (b) $PrBaCo_{2(1-x)}Fe_{2x}O_{6-\delta}$ (i.e. PBCF82 and PBCF55). Red lines marks the ranges of the working potential (on standard hydrogen electrode (SHE) potential scale) for the oxygen evolution reaction (OER) in at pH 13 used during the operando XAS study.

The indicated red lines mark the working potential range used for studying oxygen evolution reaction (OER) activity. The marked phases of $PrBaCo_2O_{6-\delta}$ (PBC) and $PrBaCo_{2(1-x)}Fe_{2x}O_{6-\delta}$ ($x \geq 0.5$) (i.e. PBCF82 and PBCF55) are phase 8 of Figure S2a ($Pr(OH)_2^{+}_{(aq)}$ + $BaOH^{++}_{(aq)}$ + $CoO(OH)^{-}_{(aq)}$) and phase 10 of Figure S2b ($Pr(OH)_2^{+}_{(aq)}$ + $Ba^{++}_{(aq)}$ + FeCo), respectively. Note that PBCF82 and PBCF55 both show the same stable phases at equilibrium. As indicated in their respective phases, all of the layered double perovskite catalysts seem to be thermodynamically unstable at equilibrium. This points out that the layered double perovskite catalysts would undergo cation dissolution. Therefore, its' initial intrinsic properties are attenuated as they reach equilibrium when in contact with aqueous solution at the indicated pH level. Ultimately, these layered double perovskite catalyst would be completely dissociated in aqueous solution remaining in those respective stable phases as indicated in the diagram; thus, the perovskite properties would be no longer present. However, it is important to emphasize that these thermodynamically stable phases are at equilibrium; in another words, the degradation as anticipated in the Pourbaix diagram is not an immediate process. Thus, OER performances of these catalysts would depend on their degradation mechanisms as dissolution is certainly also a kinetic process.

S4. Estimation of Oxygen Vacancy

A better understanding of the functional role of Fe if we were to quantify of oxygen vacancy concentration in relation to Fe content. XANES can be used to estimate the oxidation states of the perovskite cations for the calculation of oxygen content. In our previous study,[1] the oxygen content of PBC prepared by the conventional sol-gel (SG) method has been estimated by neutron diffraction, which estimated its empirical formula of $PrBaCo_2O_{5.523}$ (δ = ~0.477). Recently, we have showed that PBC produced from sol-gel method and flame spray synthesis showed differences in their physiochemical properties, such as in their oxidation states (inferred from XANES spectra) and their geometric structures (FT-EXAFS spectra).[2] Likewise, Figure S3 shows the comparison between the Co K-edge XANES spectra of PBC SG and PBC and PBCFs produce by flame spray synthesis. Figure S3 reveals that PBC SG exhibits its Co K-edge energy position at a higher energy than the perovskites produced by flame spray synthesis. From this, we can qualitatively estimate that the perovskites produced by flame spray synthesis are in lower oxidation state, which also suggests higher oxygen vacancy concentrations than that of PBC SG (δ > ~0.477); more specifically in the order of increasing oxygen vacancy: PBC < PBCF82 < PBCF55. Thus, it is reasonable that the oxygen vacancy concentration increases with increasing Fe content.

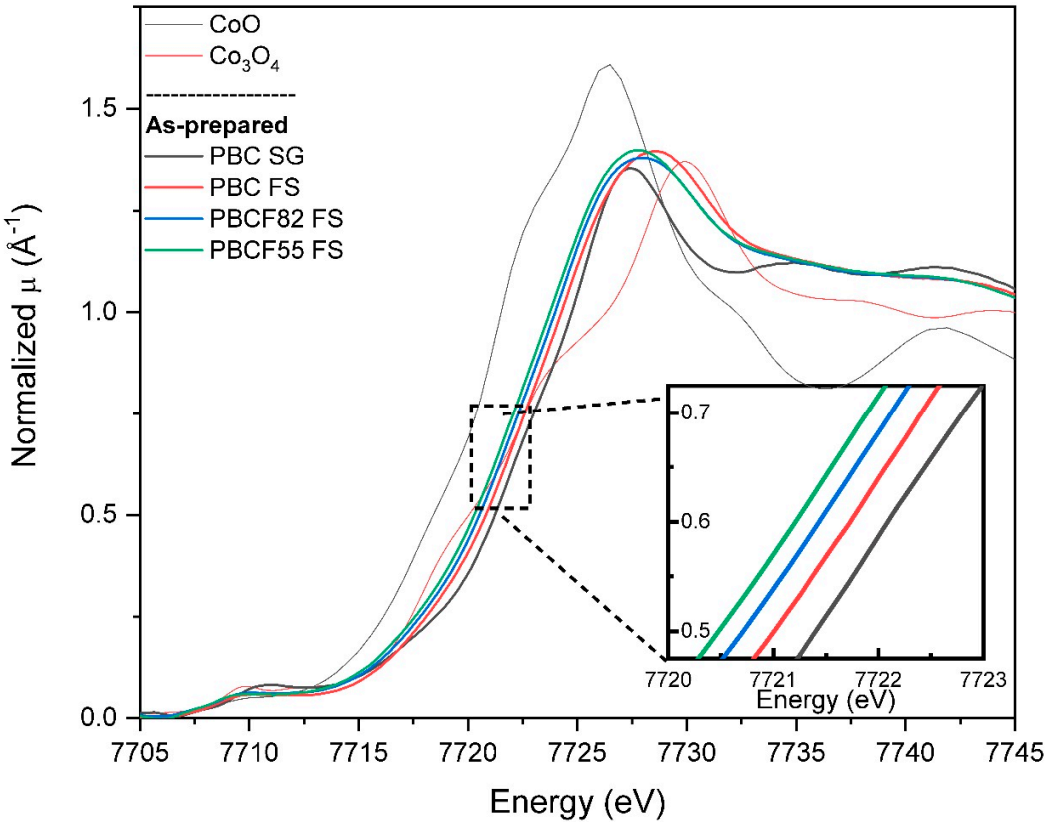

Figure S3. Comparison of XANES spectra of PBC prepared via sol-gel (SG) method (black) and PBC (red), PBCF82 (blue), and PBCF55 (green) prepared via flame spray synthesis.

S5. Lattice Parameters: Edge-sharing polyhedra and oxy(hydroxide) layer

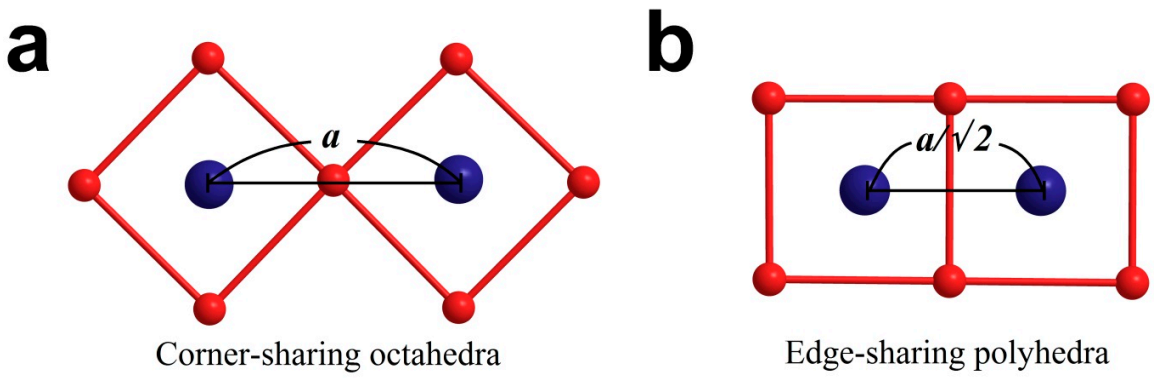

Figure S4. Illustration of Co–Co distances in (a) Co octahedra, surrounded by six oxygen atoms in an octahedral structure sharing a single oxygen corner in a typical stoichiometric perovskite (ABO_3 / $A'A''B'B''O_6$); and (b) B-site cation surrounded by less oxygen than stoichiometry ($ABO_{3-\delta}$ / $A'A''B'B''O_{6-\delta}$); therefore, the network of polyhedra would stabilize by pivoting to share two oxygen atoms.

Table S2. Lattice parameters of PBC, PBCF82, and PBCF55 calculated from Rietveld refinement of their X-ray diffractions. With the estimated lattice parameter, the Co–Co distance of edge-sharing polyhedron is calculated.

Perovskite Oxide	***a*** **Co-Co/Fe corner-shared octahedron (Å)**	***a'*** **Calculated Co-Co/Fe edge-shared polyhedron (Å)**
PBC	3.87655	2.741
PBCF82	3.88912	2.750
PBCF55	3.95297	2.795

Rietveld refinement of the X-ray diffraction (XRD) of the prepared catalysts consolidates the increase of lattice parameters as more Fe is incorporated into the B-site of layered double perovskite (Table S2). Note that the prepared catalysts are nanoparticles which render broadened XRD peaks limiting the refinement to attain precise lattice parameter estimates. Nevertheless, the increase of *a* parameter supports larger lattice parameters of Fe-doped perovskite as their XRD peaks appeared at a lower 2-theta angle than the non-doped PBC. As the layered double perovskite structure withstands even in different Co and Fe compositions, the FT-EXAFS spectra of prepared layered double perovskites would reveal similar patterns of profiles to one another. Given that all of their XRD profiles are well indexed to those characteristic of $PrBaCo_2O_{6-\delta}$ (P4/mmm) [JCPDS 00-053-0131] ($a=b\neq c$), the calculated parameters from the Rietveld refinement (*a* value) corresponds to the Co–Co distance of the corner-sharing polyhedra in the perovskite oxide.

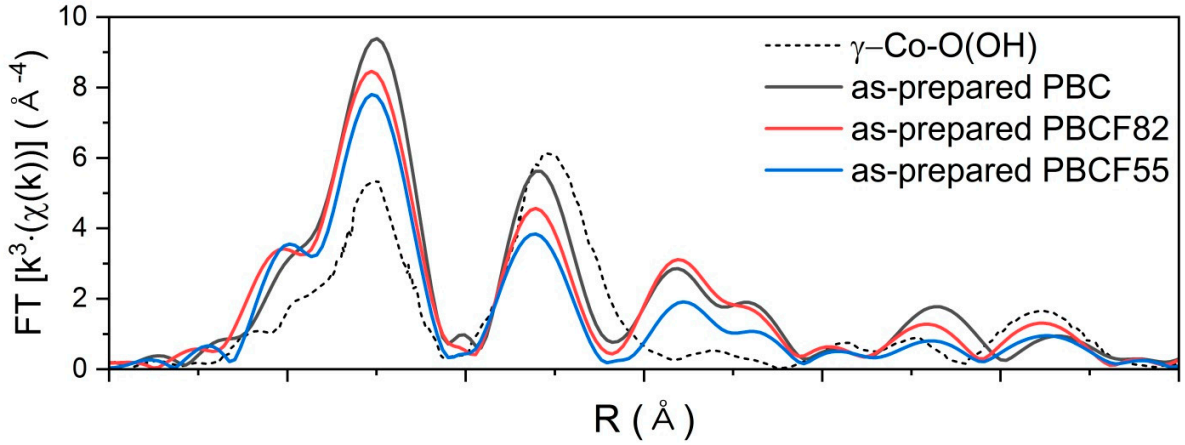

Figure S5. Comparison of Fourier transformed (FT) k^3-weighted EXAFS profiles at Co K-edge of γ-Co-O(OH)[3] with as-prepared layered double perovskite catalysts : PBC (black), PBCF82 (red), and PBCF55 (blue).

In the presence of oxygen non-stoichiometry within perovskite structure for having a high concentration oxygen vacancy, the B-site metal octahedra would be reorganized to create a more stable network by rearranging neighboring polyhedra to share its oxygen edges.[4] Consequently, the distance between Co–Co is shortened as illustrated in Figure S4b. The Co–Co distance in the edge-sharing polyhedra are calculated by a simple trigonometry ($a' = a/\sqrt{2}$) and summarized in Table S2. Coincidentally, the estimated Co–Co distances of the edge-sharing polyhedra of these layered double perovskites are close to that of Co-oxy(hydroxide) (~2.8 Å).[3,5,6] Consequently, this coinciding Co–Co distances between the edge-sharing polyhedra and Co-oxy(hydroxide) limits our interpretation of the changes observed in FT-EXAFS spectra under the operando conditions (see Figure S5).

S6. Operando FT-EXAFS Spectra Fittings

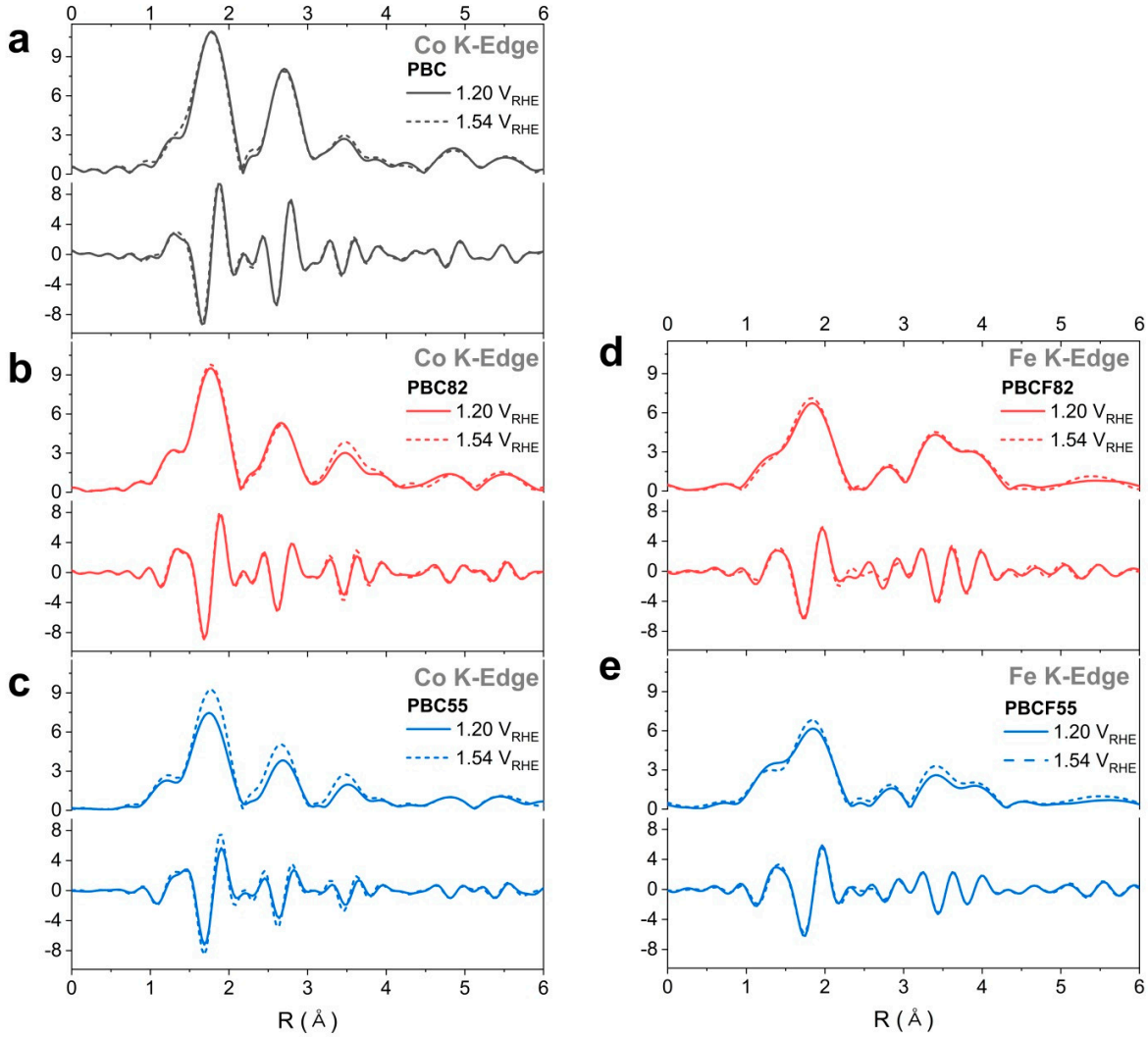

Figure S6. Comparison of FT Co K-edge EXAFS spectra collected at 1.20 and 1.54 V_{RHE} during the operando XAS measurements of (a) PBC, (b) PBCF82, and (c) PBCF55. Simultaneously collected Fe K-edge EXAFS spectra of (d) PBCF82 and (e) PBCF55.

The EXAFS spectra of PBC, PBCF82, and PBCF55 obtained during the operando flow cell tests (see Figure S6) were fitted using the Demeter software. Considering the EXAFS spectra equation below:[7]

$$\chi(k) \propto \psi_{back.sc.}(0) = \sum_j \frac{S_0^2 * N_j * f_j(k) * e^{\frac{-2R_j}{\lambda(k)}} * e^{-2k^2\sigma_j^2}}{kR_j^2} \sin\left[2kR_j + \delta_j(k)\right] \qquad \textbf{Equation S1}$$

where $f_j(k)$, $\delta_j(k)$ and $\lambda(k)$ are scattering amplitude, phase shift, and mean-free path of photoelectrons, respectively, which depend on the absorber and backscatter atom and could be obtained from the theoretical model of a scattering pair. N_j, R_j, and σ_j are structural parameters which would represent number of atoms in a shell j, radial distance from shell j, and mean square disorder of shell j at R, respectively. Finally, S_0^2 is amplitude reduction factor which is a non-structural parameter.

S_0^2 values were obtained from fitting the FT-EXAFS spectra of reference metal (i.e. Co(0)) that is collected simultaneously with the FT-EXAFS spectra of each catalyst during the operando XAS study. The theoretical model were generated from Co-metal[8] to fit the reference metal. Subsequently, this S_0^2 from fitting of each reference FT-EXAFS spectrum is used for fitting the rest of FT-EXAFS spectra of each respective perovskite catalyst.

Upon Fe incorporation, a certain level of distortion within the structure is created. Consequently, this causes reduction of amplitude peaks in FT-EXAFS spectra that display contributions of scattering from the neighboring atoms farther out in radial distance from the absorbing atoms.[9-17] Therefore, the first peak (i.e. corresponds to Co–O) is fitted using the theoretical model generated from CoOOH[18] to verify the reduction of Co oxidation states when a higher ratio of Fe is incorporated. In addition, the FT-EXAFS profiles collected at 1.2 and 1.54 V_{RHE} are also fitted to read any related changes. All of FT-EXAFS spectra were fitted in the range of 1- 2 Å. Table S3 summarizes the best fit parameters.

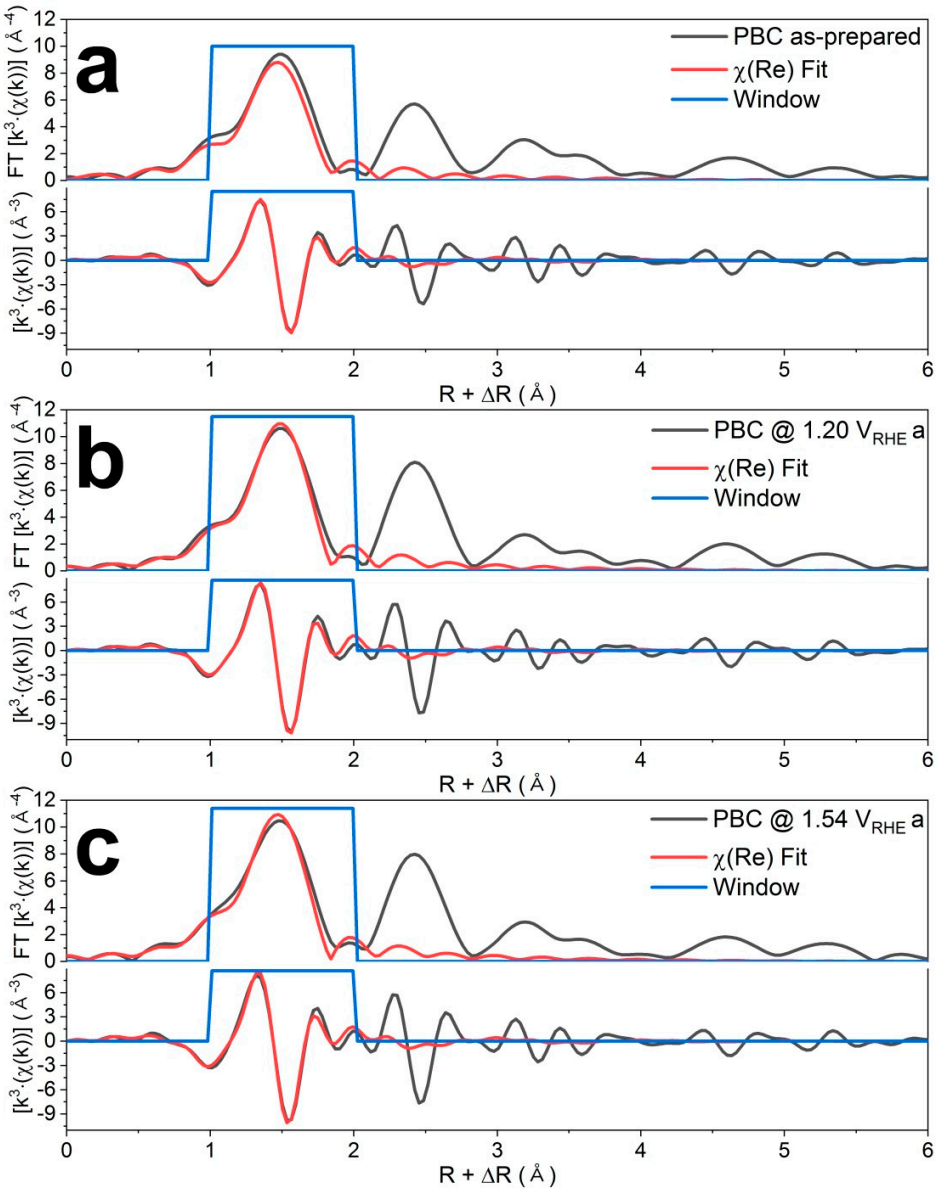

Figure S7. Fourier transformed k^3-weighted Co K-edge EXAFS spectra of PBC (a) as-prepared, (b) at 1.2 V_{RHE} anodic, and (c) 1.54 V_{RHE} anodic. Black line is the FT-EXAFS spectrum, red line is the fitted spectrum, and blue is the window of the fitting.

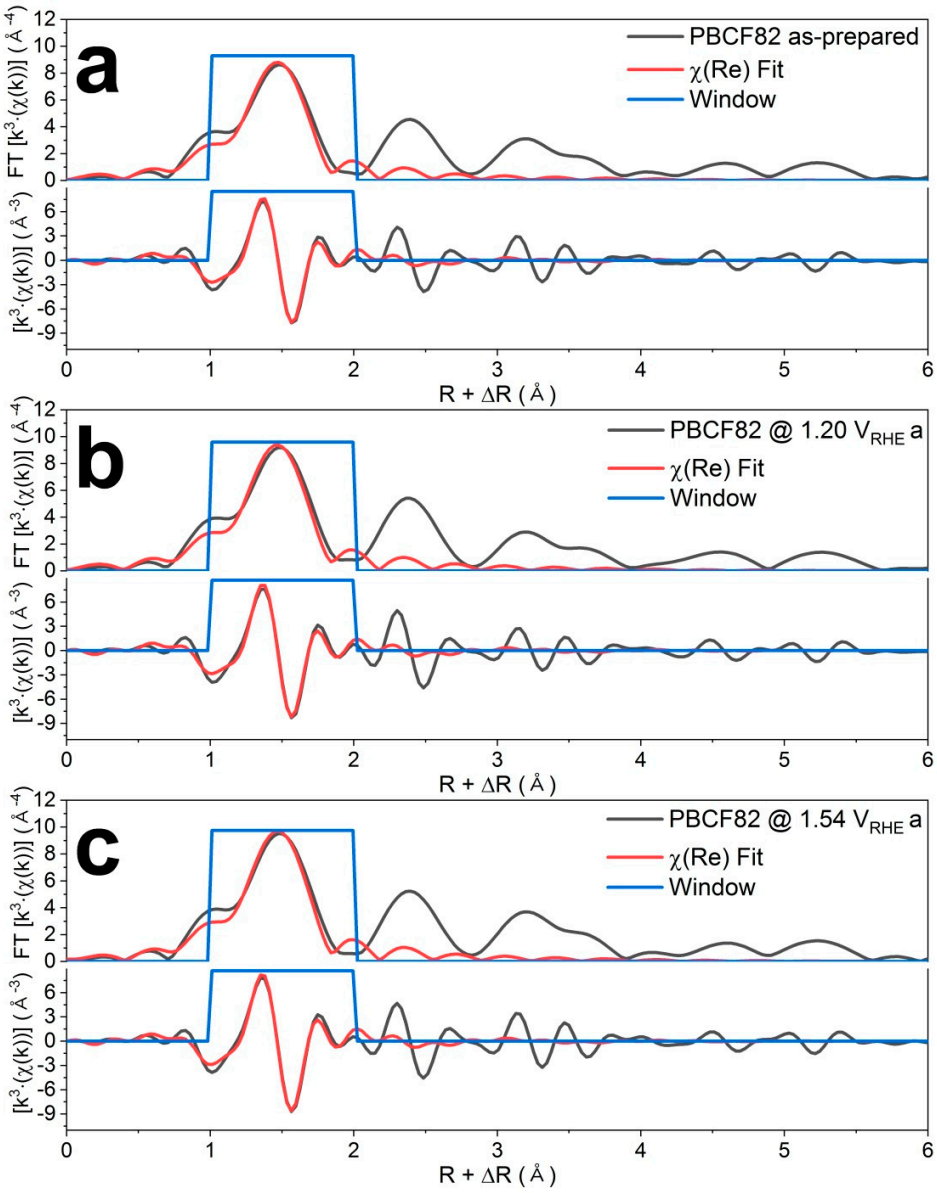

Figure S8. Fourier transformed k^3-weighted Co K-edge EXAFS spectra of PBCF82 (a) as-prepared, (b) at 1.2 V_{RHE} anodic, and (c) 1.54 V_{RHE} anodic. Black line is the FT-EXAFS spectrum, red line is the fitted spectrum, and blue is the window of the fitting.

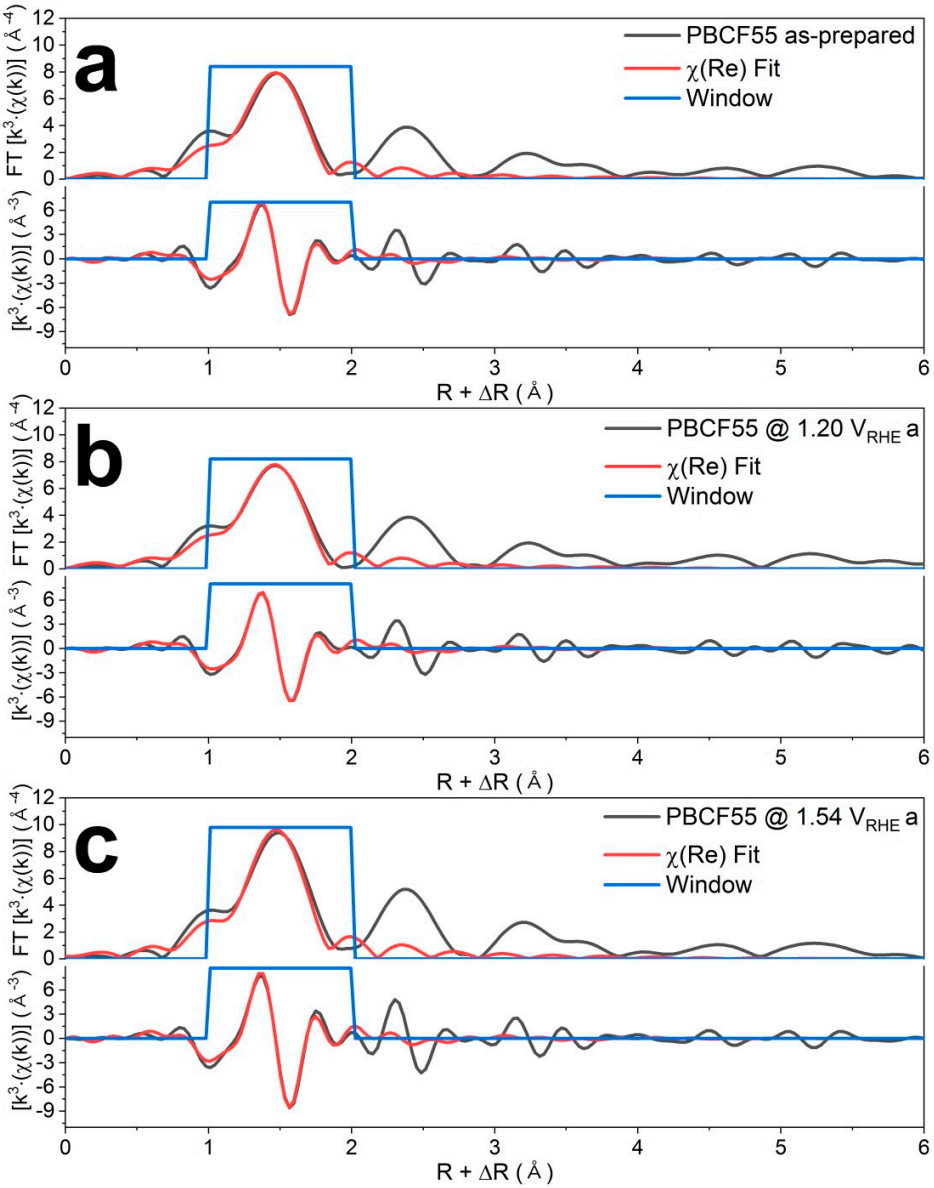

Figure S9. Fourier transformed k^3-weighted Co K-edge EXAFS spectra of PBCF55 (a) as-prepared, (b) at 1.2 V_{RHE} anodic, and (c) 1.54 V_{RHE} anodic. Black line is the FT-EXAFS spectrum, red line is the fitted spectrum, and blue is the window of the fitting.

Table S3. Summary of best fit parameters of the FT k^3-weighted Co K-edge EXAFS spectra of as-prepared and at 1.20 and 1.54 V_{RHE} during the anodic polarization of (a) PBC, (b) PBCF82, and (c) PBC55.

	Perovskite Catalysts	Potentials	Co-O				R*
			N_{Co-O}	R(Å)	σ^2(Å)^2	ΔE_0	
a	PBC	as-prepared	5.6(0.6)	1.91(0.011)	0.005(0.001)	-1(1)	0.006
		1200 mV A	5.6(0.6)	1.91(0.008)	0.004(0.001)	-0(2)	0.009
		1540 mV	6.0(0.7)	1.90(0.005)	0.005(0.005)	-1(2)	0.006
b	PBCF82	as-prepared	5.0(0.8)	1.91(0.010)	0.004(0.002)	-5(2)	0.010
		1200 mV A	5.2(0.8)	1.90(0.006)	0.004(0.002)	-5(2)	0.010
		1540 mV	5.3(0.8)	1.91(0.008)	0.004(0.002)	-4(2)	0.010
c	PBCF55	as-prepared	4.8(0.7)	1.91(0.011)	0.005(0.002)	-5(2)	0.009
		1200 mV A	5.0(0.7)	1.91(0.012)	0.005(0.002)	-6(2)	0.008
		1540 mV	5.0(0.8)	1.91(0.004)	0.004(0.002)	-4(2)	0.010

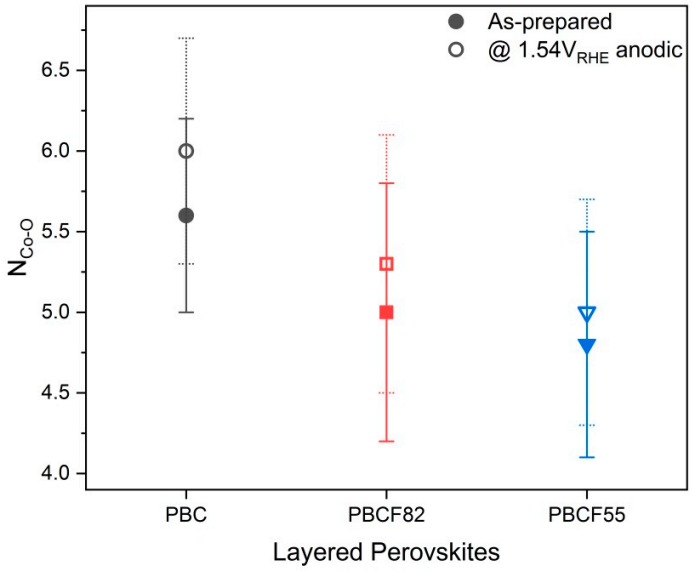

Figure S10. Comparison of coordination number (N_{Co-O}) of the first peak of FT-EXAFS spectra of PBC (black), PBCF82 (red), and PBCF55 (blue). Filled markers and empty markers represent N_{Co-O} of the as-prepared catalysts and at 1.54V_{RHE} during the anodic polarization, respectively.

Referring to Table S3 and Figure S10, smaller N_{Co-O} values are estimated with increasing the Fe composition. This consolidates that Co is indeed coordinated with less oxygen upon Fe incorporation. Therefore, PBCF55, the one with the highest amount of Fe-doping, revealed the smallest Co–O coordination number (4.8), while in the absence of Fe (i.e. PBC) showed the highest Co–O coordination number (6.0).

Despite each perovskite showed different extent of edge shifts during the anodic polarization (Figure 5b), this is not clearly manifested in the corresponding N_{Co-O} values at 1.54 V_{RHE}. For instance, PBC and PBCF55 each revealed an edge shift of ~0.3 eV and ~0.7 eV, respectively; however, increases in their N_{Co-O} at 1.54 V_{RHE} are similar. This is presumably due to having both Co dissolution and oxidation occurring simultaneously during the anodic polarization, where each has opposing effects in the first peak amplitude of FT-EXAFS spectra. Nevertheless, some deductions can still be made considering the clear Co K-edge

position shifts shown by XANES spectra: i) Co is oxidized during the OER process, ii) while cations are dissolved at different rate which is governed by their kinetics.

References

1. Cheng, X.; Fabbri, E.; Yamashita, Y.; Castelli, I.E.; Kim, B.; Uchida, M.; Haumont, R.; Puente-Orench, I.; Schmidt, T.J. Oxygen evolution reaction on perovskites: A multieffect descriptor study combining experimental and theoretical methods. *ACS Catal.* **2018**, *8*, 9567-9578.
2. Kim, B.J.; Cheng, X.; Abbott, D.F.; Fabbri, E.; Bozza, F.; Graule, T.; Castelli, I.E.; Wiles, L.; Danilovic, N.; Ayers, K.E., *et al.* Highly active nanoperovskite catalysts for oxygen evolution reaction: Insights into activity and stability of ba0.5sr0.5co0.8fe0.2o2+delta and prbaco2o5+delta. *Adv. Funct. Mater.* **2018**, *28*.
3. Huang, J.H.; Liu, Q.H.; Yao, T.; Pan, Z.Y.; Wei, S.Q. Xafs study on structure-activity correlations of alpha-co(oh)(2) nanosheets water oxidation catalysts. *J. Phys. Conf. Ser.* **2016**, *712*, 012128.
4. Gibb, T.C. Evidence for an unusual phase in the perovskite-related system bacoxmn1-xo3-y from exafs spectroscopy. *J. Mater. Chem.* **1992**, *2*, 387-393.
5. Huang, J.H.; Shang, Q.C.; Huang, Y.Y.; Tang, F.M.; Zhang, Q.; Liu, Q.H.; Jiang, S.; Hu, F.C.; Liu, W.; Luo, Y., *et al.* Oxyhydroxide nanosheets with highly efficient electron-hole pair separation for hydrogen evolution. *Angew. Chem. Int. Edit.* **2016**, *55*, 2137-2141.
6. Totir, D.; Mo, Y.B.; Kim, S.; Antonio, M.R.; Scherson, D.A. In situ cok-edge x-ray absorption fine structure of cobalt hydroxide film electrodes in alkaline solutions. *J. Electrochem. Soc.* **2000**, *147*, 4594-4597.
7. Rehr, J.J.; Albers, R.C. Theoretical approaches to x-ray absorption fine structure. *Rev. Mod. Phys.* **2000**, *72*, 621-654.
8. Kulesko, G.I.; Seryugin, A.L. Geometrical shape of martensite plates in cobalt. *Phys. Metals. Metallog.* **1968**, *26*, 140.
9. Gorlin, M.; Chernev, P.; de Araujo, J.F.; Reier, T.; Dresp, S.; Paul, B.; Krahnert, R.; Dau, H.; Strasser, P. Oxygen evolution reaction dynamics, faradaic charge efficiency, and the active metal redox states of ni-fe oxide water splitting electrocatalysts. *J. Am. Chem. Soc.* **2016**, *138*, 5603-5614.
10. Gangopadhayay, S.; Inerbaev, T.; Masunov, A.E.; Altilio, D.; Orlovskaya, N. Structural characterization combined with the first principles simulations of barium/strontium cobaltite/ferrite as promising material for solid oxide fuel cells cathodes and high-temperature oxygen permeation membranes. *ACS Appl. Mater. Interfaces* **2009**, *1*, 1512-1519.
11. Ganopadhyay, S.; Masunov, A.E.; Inerbaev, T.; Mesit, J.; Guha, R.K.; Sleiti, A.K.; Kapat, J.S. Understanding oxygen vacancy migration and clustering in barium strontium cobalt iron oxide. *Solid State Ionics* **2010**, *181*, 1067-1073.
12. Mueller, D.N.; De Souza, R.A.; Brendt, J.; Samuelis, D.; Martin, M. Oxidation states of the transition metal cations in the highly nonstoichiometric perovskite-type oxide ba0.1sr0.9co0.8fe0.2o3-delta. *J. Mater. Chem.* **2009**, *19*, 1960-1963.
13. Arnold, M.; Xu, Q.; Tichelaar, F.D.; Feldhoff, A. Local charge disproportion in a high-performance perovskite. *Chem. Mater.* **2009**, *21*, 635-640.
14. Jun, A.; Kim, J.; Shin, J.; Kim, G. Perovskite as a cathode material: A review of its role in solid-oxide fuel cell technology. *ChemElectroChem* **2016**, *3*, 511-530.
15. Kuklja, M.M.; Kotomin, E.A.; Merkle, R.; Mastrikov, Y.A.; Maier, J. Combined theoretical and experimental analysis of processes determining cathode performance in solid oxide fuel cells. *Phys. Chem. Chem. Phys.* **2013**, *15*, 5443-5471.
16. Glazer, A.M. Simple ways of determining perovskite structures. *Acta Crystallogr., Sect. A* **1975**, *31*, 756-762.
17. Risch, M. Perovskite electrocatalysts for the oxygen reduction reaction in alkaline media. *Catalysts* **2017**, *7*.

18. Delaplane, R.G.; Ibers, J.A.; Ferraro, J.R.; Rush, J.J. Diffraction and spectroscopic studies of cobaltic acid system hcoo2-dcoo2. *J. Chem. Phys.* **1969**, *50*, 1920-1927.